Varying Lithospheric Thickness Controls Mantle and Crustal Deformation in Western U.S.

Zebin Cao, Lijun Liu

Department of Geology, University of Illinois at Urbana-Champaign, Urbana, IL

Introduction

The crustal deformation within the tectonically active western U.S. (WUS) has a complex spatial pattern, whose driving mechanism remains debated. We suggest that one important reason behind these debates is the lack of a clear understanding on the lithosphere-asthenosphere interaction in this region. We construct a data-orientated geodynamic model with detailed lithospheric and mantle dynamics, all computed within one single dynamic system, based on which we quantify the relative importance of different mechanisms in driving intracontinental deformation in the WUS, particularly the previously unexplored lithosphere-asthenosphere interaction.

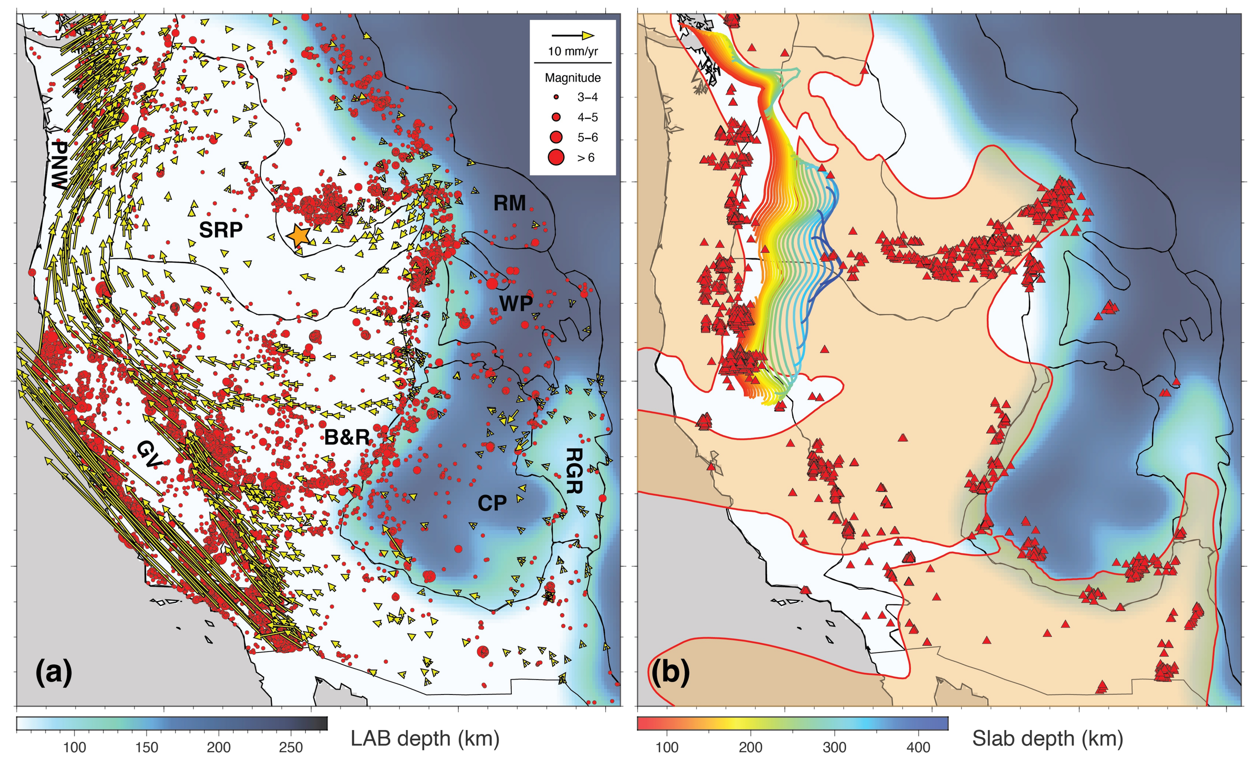

Figure 1. Crustal deformation, lithosphere thickness, intraplate volcanoes, slab geometry, and hot asthenospheric material below the WUS. (a) Seismicity and geodetically measured crustal motion overlying the lithosphere-asthenosphere boundary (LAB) depth. Red dots indicate earthquake locations during the past 40 years, with radius showing magnitudes. Yellow arrows indicate crustal motion relative to the stable North American plate determined with GPS measurements. The orange star in the central Idaho approximates the rotation center of the WUS crustal motion. (b) Intraplate volcanism during the past 2 Myrs (red triangles), slab surface (colored contours indicate depths), and hot asthenospheric material (orange regions with red outlines representing a temperature 30˚C warmer than the ambient mantle) at 100 km depth overlying the LAB depth. Thin black lines in both panels indicate major tectonic provinces in the WUS.

Geodynamic Modeling Approach

We utilize a newly constructed geodynamic modeling approach to simultaneously study the WUS lithospheric and asthenospheric deformation (Cao & Liu, 2021). In this model, the buoyancy structure of the convecting mantle is based on a hybrid data-assimilation approach that satisfies multiple geophysical and geological observations in the region (Zhou & Liu, 2017, 2019; Zhou *et al.*, 2018a, 2018b). We then combine this mantle structure with the seismically inferred crust and lithospheric mantle to reproduce the observed crustal stress state, surface velocity field, and asthenospheric flow consistent with observed anisotropy.

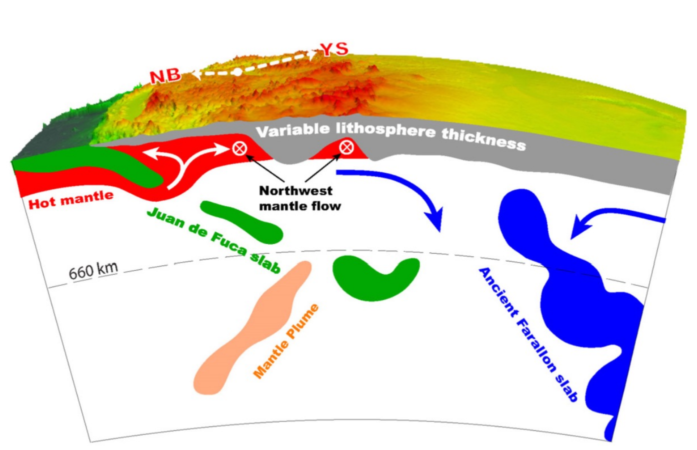

Figure 2. Schematics for the lithospheric and mantle structures in the fully coupled lithosphere-mantle geodynamic model. We applied plate motion in surrounding ocean basins to incorporate the far-field forces, while set the continent to be free-slip. Lithospheric and mantle dynamics are simultaneously computed in one physical frame.

Predicted Mantle and Lithospheric Dynamics in the WUS

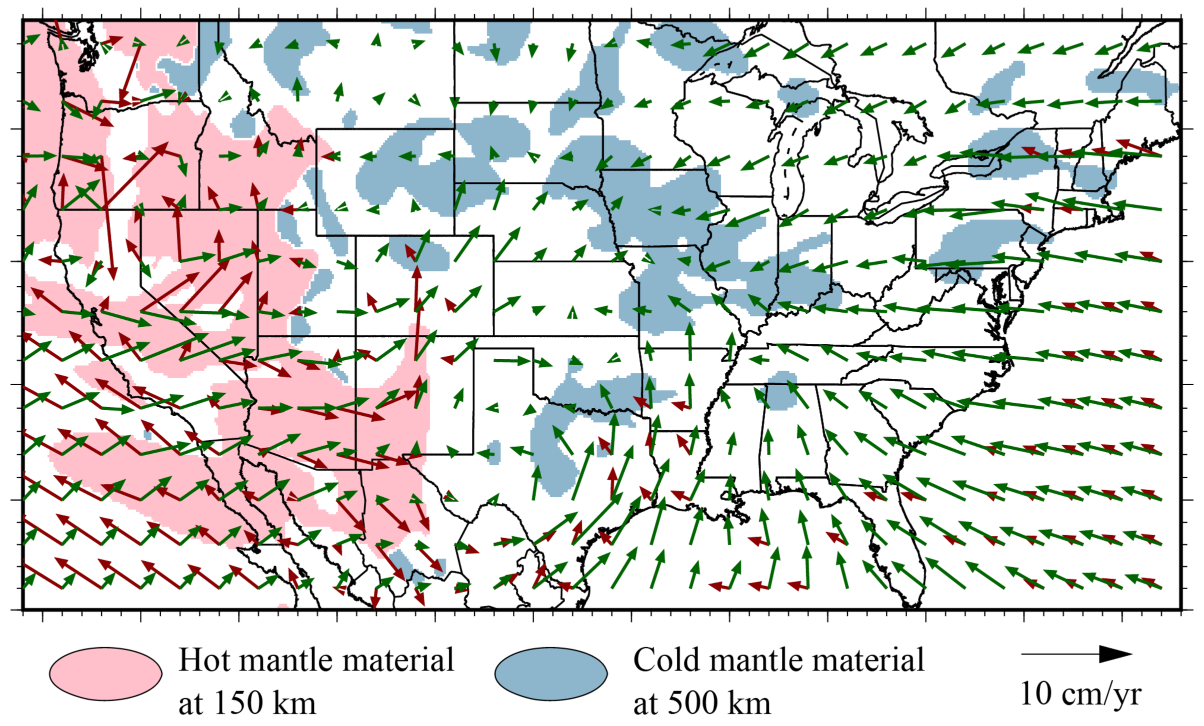

Figure 3. Downward view of mantle flow (arrows) and major thermal anomalies (contours). The intruding hot oceanic mantle (pink contour, at 150 km) driven by the sinking Farallon slab on the east interacts with the lithosphere causing complex mantle flow (red arrows, at 150 km). Sinking of cold anomalies including the Farallon slab (blue contour, at 500 km) drives the large-scale E-W flow (green arrows, at 300 km).

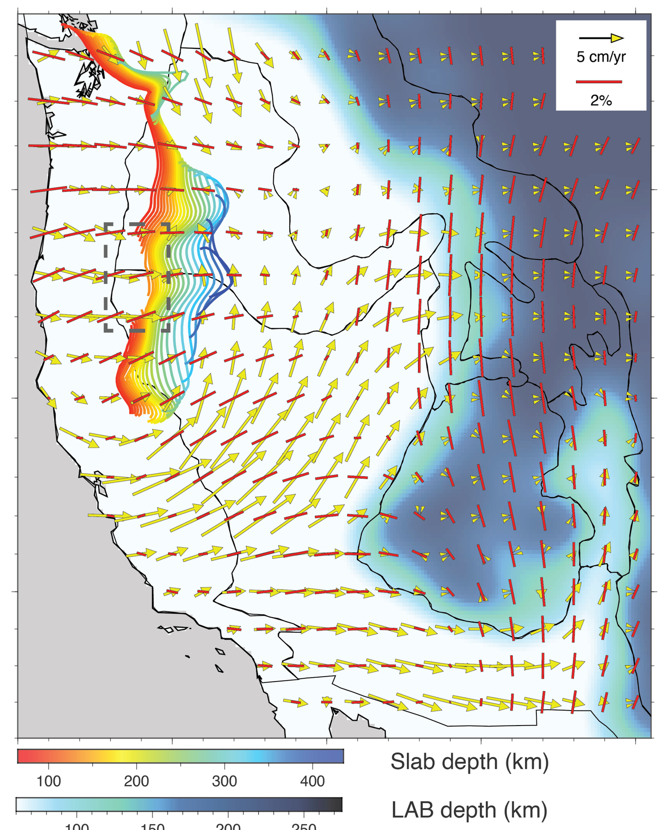

Figure 4. Slab surface (colored contours indicate depths), predicted mantle flow at 150 km (yellow arrows, relative to stable North American plate), and azimuthal seismic anisotropy at 100 km (red bars show the fast-propagating direction of shear waves, Zhu et al., 2020) overlying the LAB depth. The segmented slab surface within the dashed black box represents a slab tear, which allows hot asthenospheric material to flow through. The predicted mantle flow pattern is vividly tracking the azimuthal anisotropy below the thin WUS lithosphere.

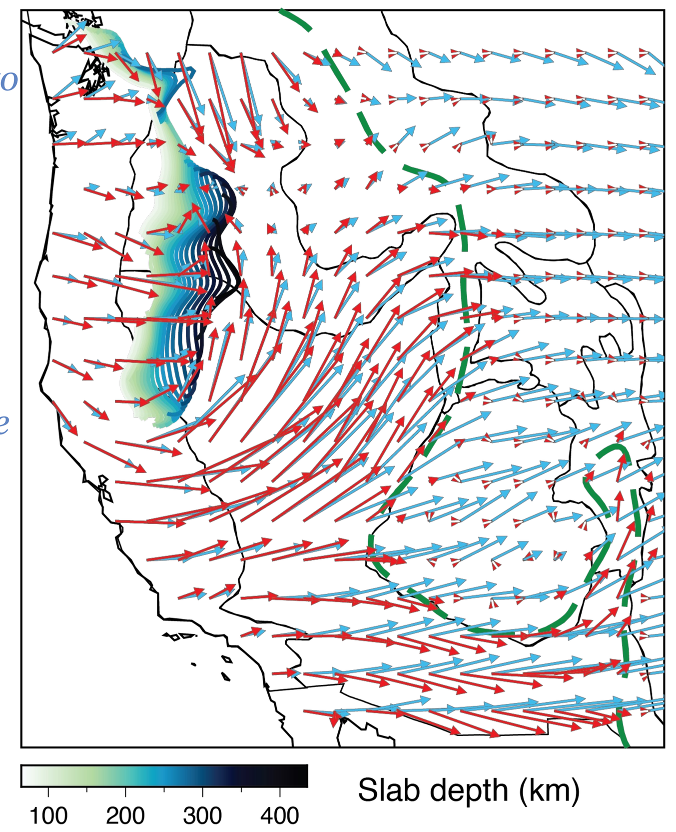

Figure 5. Comparison of predicted mantle flow relative to stable North American plate at 150 km between the model with constant lithosphere thickness (light-blue arrows) and the model with lateral varying lithosphere thickness (red arrows). The colored contours indicate the upper surface of the slab at different depths. The dark-green dashed line marks the location of LAB at 75 km, which approximates the transition from thin to thick lithosphere. With lateral varying lithosphere thickness, the mantle flow is confined in the tectonically active WUS.

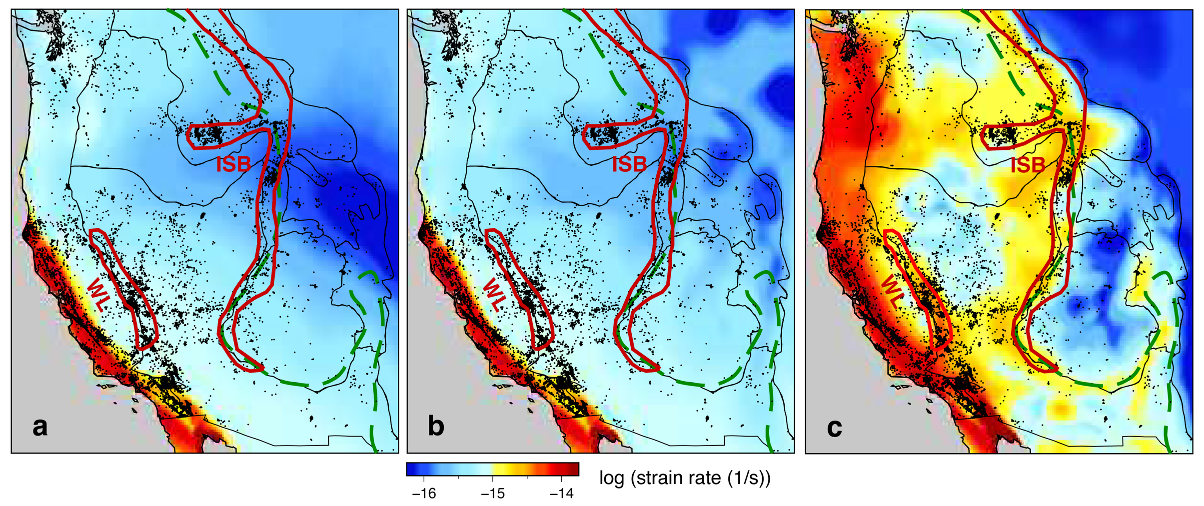

Figure 6. Predicted second invariant of depth-averaged crustal strain rate in the uppermost 30 km with (a) a uniform lithosphere, (b) a lithosphere same as in (a) but with varying Moho depth, (c) a heterogeneous lithosphere as seismically inferred. Black dots in (a) – (c) indicate earthquake locations in the past 40 years. The thick red lines in (a) - (c) outline the Walker Lane (WL) and the Intermountain Seismic Belt (ISB).

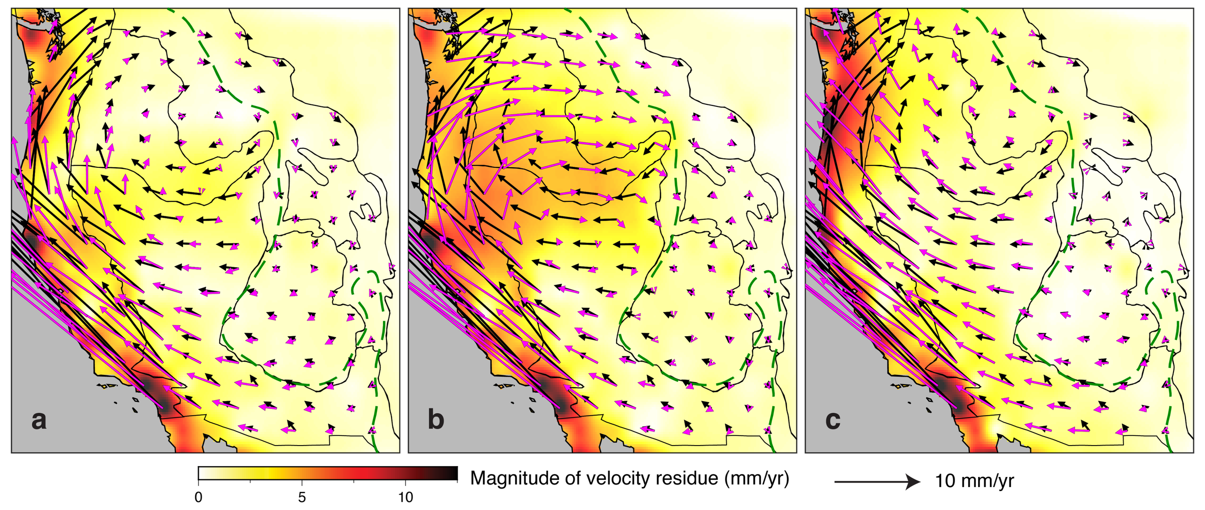

Figure 7. Predicted crustal motion with (a) plate boundary forces only, (b) plate boundary forces and basal traction, (c) plate boundary forces and lithospheric GPE. The black bars represent the smoothed GPS measurements, and the magenta bars represent the predictions.

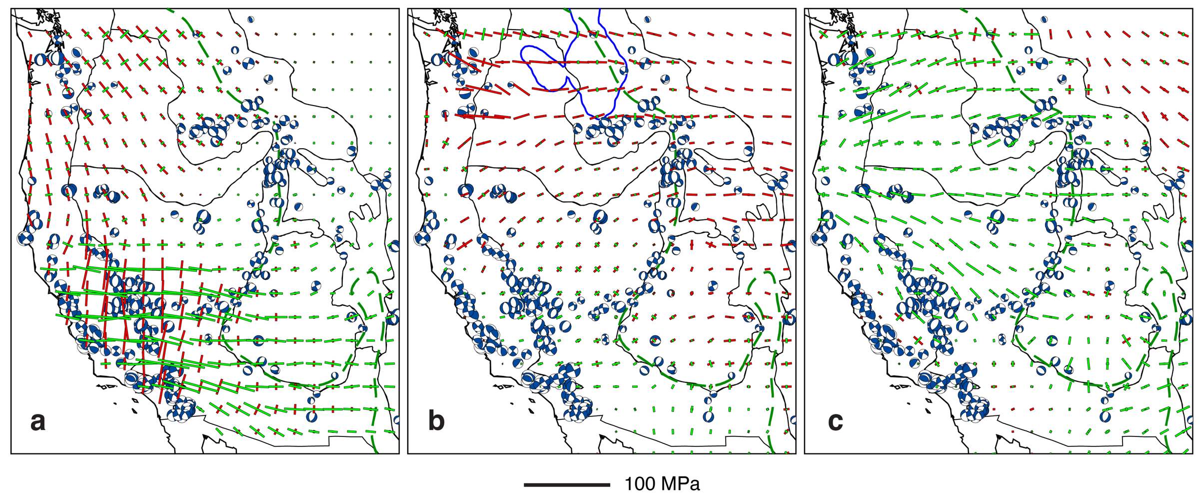

Figure 8. Predicted crustal stress with different driving forces overlying observed focal mechanism solutions. Predicted crustal stress due to (a) plate boundary forces, (b) basal traction, and (c) lateral gradients of lithospheric GPE. The bars show the directions and magnitudes of horizontal principal stresses. Red represents compression, and green represents extension. Focal mechanism solutions are from Saint Louis University Catalogue and gCMT. The purple contour in (b) outlines the slab curtain, which locally enhances basal traction, at 150 km.

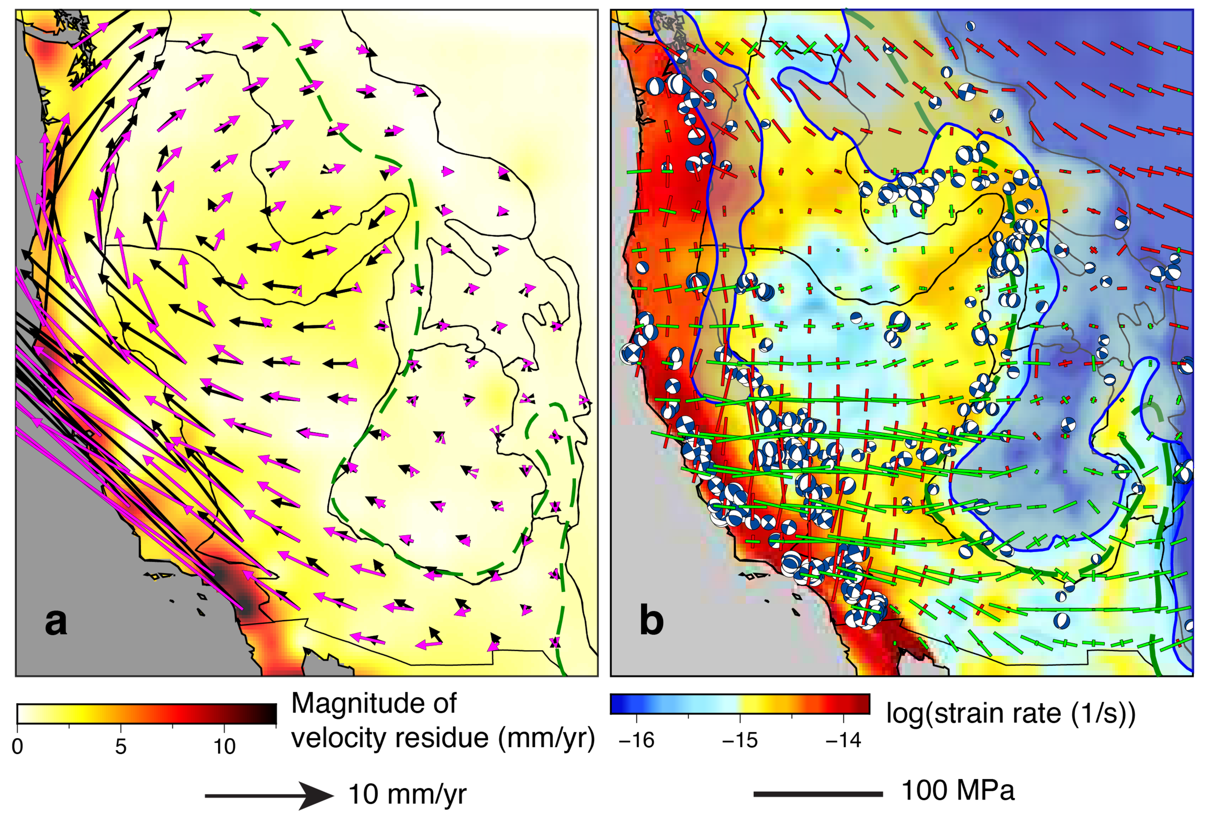

Figure 9. Predicted crustal deformation and stress driven by all driving forces combined. (a) Crustal motion driven by all driving forces combined. (b) Predicted crustal stress and observed focal mechanism solutions overlying predicted second invariant of depth-averaged crustal strain rate. The shaded regions represent cold materials, including subducting slab, slab curtain, lithospheric drips, and continental lithosphere at 100 km (with the outline representing a temperature 10 ˚C cooler than the ambient mantle). The bars show directions and magnitudes of horizontal principal stress, the same as in Fig. 8.

Crustal Deformation Driven by Lithosphere-Asthenosphere Interaction

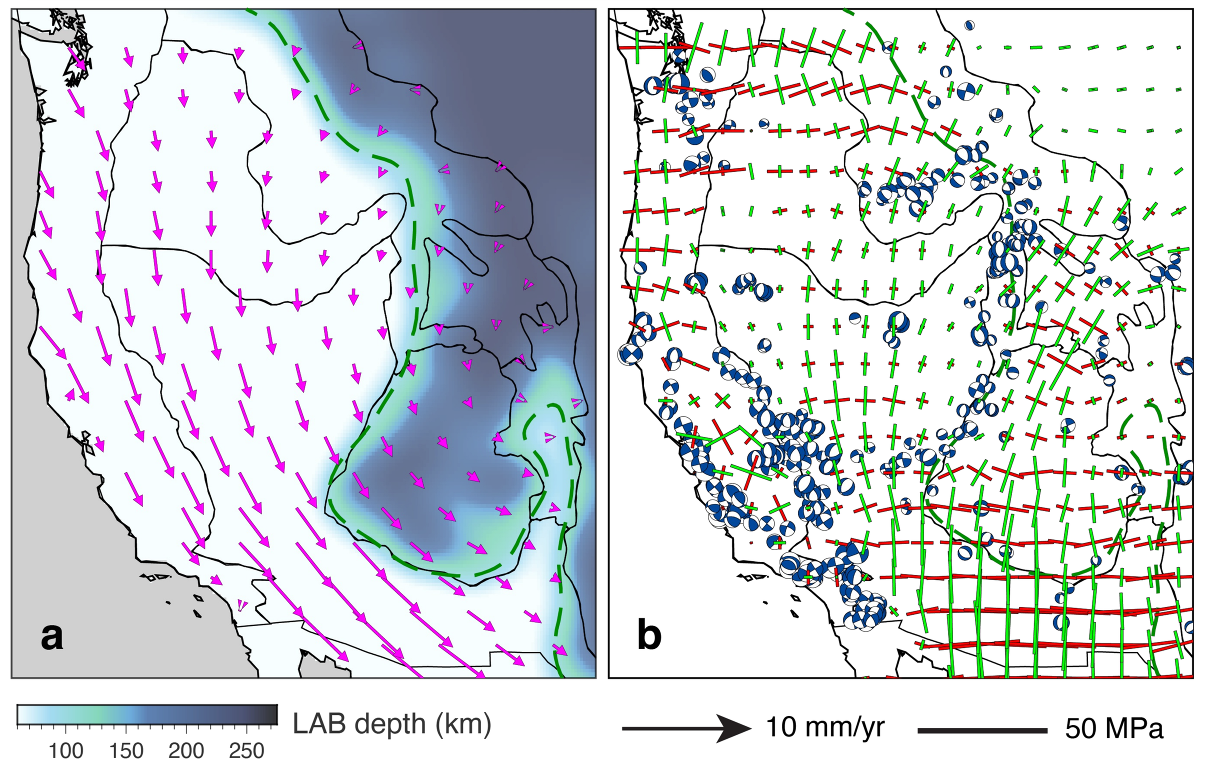

Figure 10. Predicted crustal motion and stress driven by lithosphere-asthenosphere interaction (difference between models with a varying LAB depth and a constant LAB depth). (a) WUS crustal motion driven by lithosphere-asthenosphere interaction due to varying LAB depth. (b) Crustal stress due to the geometric effect of LAB depth, overlying focal mechanism solutions. The bars show the directions and magnitudes of horizontal principal stresses, the same as in Fig. 8.

Implication for Intraplate Volcanism

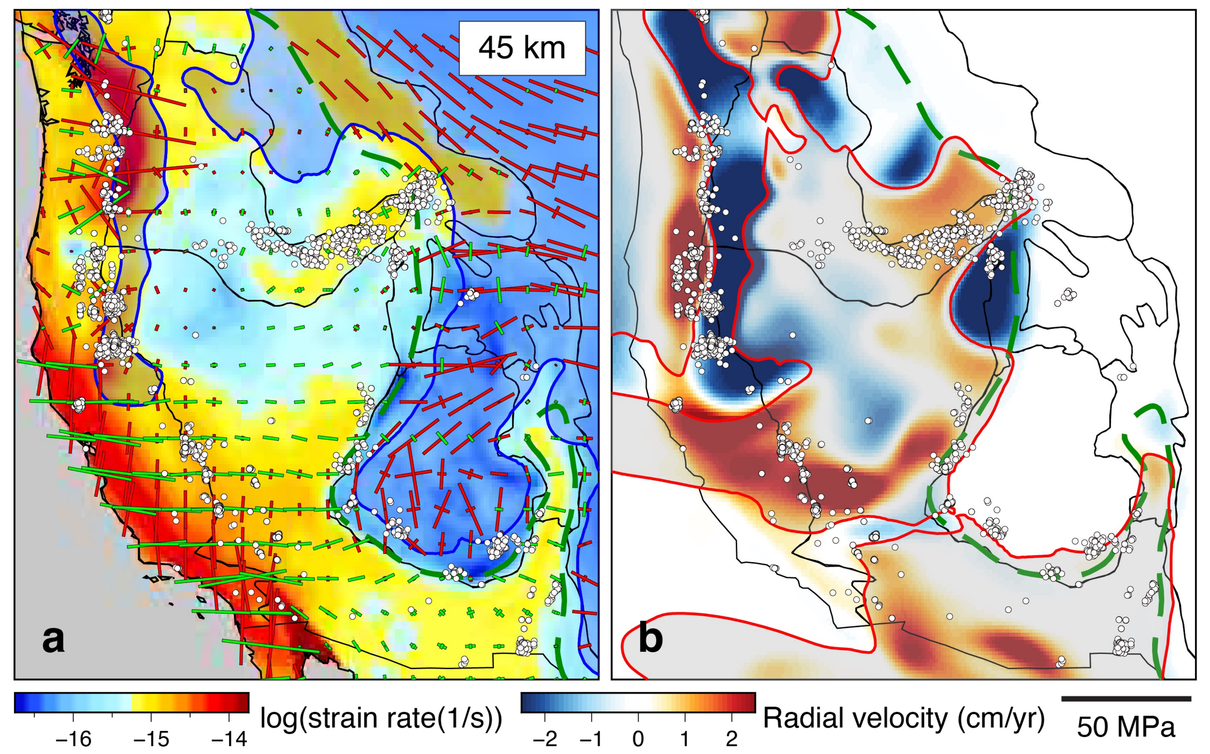

Figure 11. Lithospheric deformation and volcanisms in the WUS. (a) Predicted lithospheric mantle strain rate and recent volcanisms. The bars show directions and magnitudes of horizontal principal stress, the same as in Fig 8. The shaded regions represent cold materials, the same as in Fig 9b. (b) Radial component of the mantle flow at 100 km and volcanisms. The shaded regions with red outlines represent hot asthenospheric material, the same as in Fig 1b. The white dots in both panels indicate the locations of volcanisms during the most recent 2 Myrs.

Conclusions

1. The lithosphere-asthenosphere interaction plays a key role in defining observed WUS intraplate deformation.
2. The driving force for crustal deformation varies spatially, and the lithosphere-asthenosphere interaction affects the entire WUS, especially in forming the rotational pattern of crustal motion, spatially varying earthquake distribution and focal types, and recent intraplate volcanism.
3. Intraplate volcanism forms in regions with both strong mantle upwelling and trans-lithospheric extension.